Supplementary Material: Rock surface luminescence dating of gravel determines the age of a glacial outburst megaflood, Glacial Lake Missoula, Montana, USA

Larry N. Smith[1*], Reza Sohbati[2,3], and Mayank Jain[2]

[1]*Geological Engineering, Montana Technological University, Butte, MT 59701, USA*

[2]*Department of Physics, Technical University of Denmark, DTU Risø Campus, DK-4000, Roskilde, Denmark*

[3]*Danish National Metrology Institute, Hørsholm DK-2970, Denmark*

SAMPLING AND SAMPLE PREPARATION

About 20 cobbles were extracted for optical dating from each of three different pits more than 20 minutes after sunset. The three sample pits are all located in an active gravel quarry (2018 sample, site 1 - 47.03717°N, 114.3730°W; 2019 site 2 - 47.0362°N, 114.3746°W and 2019 site 3 - 47.0367°N, 114.3719°W). All sampled clasts were very fine- to medium-grained feldspathic quartzite and feldspathic sandstone with abundant amounts of quartz and feldspar, which are the target minerals for luminescence dating. Cobbles were wrapped in aluminium foil and placed in a light-tight bag. One sample of granule- and pebble-sized matrix was taken from around the sampled cobbles at the 2018 pit; two such samples were taken from each of two pits in 2019. Due to open-work nature of the deposit, granule-sized matrix material did not exist between all cobbles. Discontinuous and thin (< 2 mm) coatings of silt and clay were on many clasts, especially on granules and cobbles; these are most likely introduced into the gravel from suspended sediments in GLM (c.f. Mooneyham and Strom, 2018). The silt and clay coatings were scraped from the 15 cobbles from each of the 2019 pits; these two composite samples were included with the five other matrix samples for dose-rate measurements.

Cobbles with the fewest fractured faces from each pit (8 in 2018 and 30 in 2019) were selected from the ~60 rocks collected, and shipped to the Department of Physics, Technical University of Denmark, Risø Campus laboratory for measurement.

Samples for luminescence measurements were prepared under low-level amber light (Sohbati et al., 2017). Each of the cobbles was cored using a diamond-embedded, water cooled, coring bit mounted in a bench-model drill press, after Sohbati et al. (2011). Initially, ~10 mm diameter cores were drilled perpendicularly to each of the two tabular rock faces, arbitrarily designated “top” and “bottom”, to at least the center of the cobble, resulting in two cores per sample. Cores from 36 of the 38 clasts were successfully drilled from both tabular sides of each rock. Cores were sectioned into slices on a Buehler Isomet low-speed saw with a 0.3 mm-thick diamond-embedded blade at ~1 mm intervals; resulting slice thicknesses average 0.76 mm (n = 721). Slices from each core of the cobbles were mounted directly on reader carousels for discs for luminescence measurements without any further mechanical or chemical treatment (Sohbati et al., 2011).

INSTRUMENTATION AND MEASUREMENTS

Luminescence measurements

All the luminescence measurements were carried out on Risø TL/OSL DA-20 readers. The continuous-wave (CW) IRSL signals were stimulated for 100 s using infrared (IR) LEDs (λ_{max} = 850 ± 33 nm) with a Lighting Power Density (LPD) of > 300 mW.cm^{-2} at sample position and detected through a Schott BG-3/BG-39 blue filter combination (Table S1). The post-infrared CW and pulsed OSL (abbreviated as post-IR OSL and post-IR POSL, respectively; Tsukamoto and Rades, 2016) measurements were carried out on readers equipped with automated Detection And Stimulation Head (DASH, Lapp et al., 2015). The post-IR OSL signals were stimulated for 100 s subsequent to CW IR stimulations at 50 ^{o}C (and 225 ^{o}C) each for 100 s, while the post-IR POSL signals were stimulated for 160 s (Table S1). All OSL signals (CW and pulsed) were stimulated using blue LEDs (λ_{max} = 470 ± 20 nm, LPD > 80 mW.cm^{-2}) and measured through a Hoya U-340 UV filter with a total thickness of 7.5 mm. The POSL pulse durations were 200 µs during which the blue LEDs were switched on and off for 50 µs and 150 µs, respectively. The POSL signal was recorded during the off-time only (Denby et al., 2006). The aliquots were heated to 250 ^{o}C and kept at this temperature for 100 s prior to all optical stimulations (Table S1). A high temperature blue stimulation at 290 ^{o}C for 100 s was also carried out at the end of each cycle to minimize the signal carry-over to the next cycle in equivalent dose (D_e) measurements (Murray and Wintle, 2003). A heating rate of 2 or 5 ^{o}C s^{-1} was used during preheat treatments for IRSL and POSL measurements. A pause of 30 s was also inserted before the stimulations to ensure that the whole volume of the rock slices had reached the stimulation temperature (Sohbati et al., 2015). Five empty channels were put before and after each stimulation to monitor any Isothermal Thermoluminescence (ITL) signal. The irradiations were carried out using a ^{90}Sr beta source calibrated using sensitised quartzite rock slices (Sohbati et al., 2012).

A single aliquot regenerative-dose (SAR) protocol (Murray and Wintle, 2000) with a test dose of 12, 16, or 20 Gy, depending on instrument was used for both IRSL and post-IR POSL measurements (Table S1). Test doses of such sizes have been reported to be appropriate for measuring both small doses near the surface of the rock as well as large doses close to saturation at depth (Liu et al., 2016). The IRSL natural sensitivity-corrected signals (L_n/T_n) were calculated using the first 1 s (channels: 6-10) of the signals subtracted by the average of the last 10 s (channels: 446-495). The corresponding integration intervals for the calculation of post-IR POSL L_n/T_n values were 1.12 s (channels: 6-12) and 1.28 s (channels: 13-20), respectively.

Dose rate measurements

The dose rate measurements were carried out on the remaining material (~300 g) after drilling from cobbles that were identified as suitable for dating, and the material from the surrounding matrix. Each sample was crushed and pulverized, heated to 450°C for 24 h to remove any organic matter and to dehydrate minerals, and cast with wax to produce a reproducible geometry and prevent radon loss. Samples were then stored for at least 3 weeks to allow ^{222}Rn to reach equilibrium with its parent ^{226}Ra before being measured on a high-purity germanium detector for at least 24 h (Murray et al., 2018). The activity concentrations of ^{238}U, ^{232}Th, and ^{40}K were measured using the high-resolution gamma spectrometry (Murray et al., 2018) and converted to dose rate using the conversion factors by Guérin et al. (2011).

Grain size measurements

To quantify the mineralogy and grain size of cobbles C-3 and C-4, minerals were mapped at a resolution of 3 µm across polished thin sections (C-3: 13 x 27 mm; C-4: 9.5 x 19 mm) using Scanning Electron Microscopy-Energy Dispersive X-ray spectroscopy (SEM-EDX).

Matrix porosity estimation

One factor affecting the radiation dose of material surrounding the samples is the porosity of the matrix. A higher porosity sediment will reduce the effect of ionizing radiation because therefore there is less radioactive material near the sample. The porosity of the sediment matrix was estimated from a photograph of the sampling location using ImageJ (Schneider et al., 2012; Jutzeler et al., 2012). The software is used to image material versus interstitial spaces between the gravel clasts, resulting in an average porosity for the photographed outcrop.

LUMINESCENCE CHARACTERISTICS

K-rich feldspar IRSL

Quartz is the preferred dosimeter in luminescence dating (Aitken, 1985). Thus, to isolate the quartz signal from whole rock slices, eight of the least broken and more rounded cobbles that were collected from a single pit in the first field campaign in 2018 were measured using a double-SAR protocol (Banerjee et al., 2001). In this protocol the blue-stimulated OSL signal is measured after the infrared-stimulated signal (Table S1). Quartz is largely insensitive to IR stimulation, while feldspar luminescence signal can be depleted by both IR and blue stimulations (e.g. Duller, 2003). A double-SAR protocol can thus allow us to measure (and so deplete) the feldspar signal in the first stimulation step with IR, while the post-IR blue stimulated signal measured in the second step preferentially originates from quartz (Duller, 2003). The typical IRSL and post-IR OSL signals from a rock slice are shown in Fig. S1. As expected, the post-IR OSL signal depletes faster than the IRSL signal. However, a comparison between the corresponding post-IR OSL stimulation curves from a slice of sample C-4 and a sensitised calibration quartzite slice reveals that the latter signal decays even more rapidly (Fig. S1). The likely explanation for this observation is that the observed post-IR OSL signals from slices of C-3 and C-4 are contaminated with feldspar slow-decaying signal. If the IR stimulation in the first step is not sufficient to entirely deplete the signal, then the remaining feldspar signal can be stimulated by blue stimulation in the subsequent step and obscure the fast component of the quartz OSL signal. An alternative reason could be that the OSL signal from the constituent quartz in our samples does not have a fast component. Regardless of the true explanation for this observation, the post-IR OSL signal from these slices is not deemed as suitable for dating due to its composite origin or lack of fast component. Consequently, further data analyses on these samples including C-3 and C-4 were carried out using IRSL signals only.

Post-IR POSL

Additional sampling was done in 2019, where 15 cobbles each were collected from two additional pits dug at the quarry. Guided by the results from 2018 samples, we followed a more rigorous approach to separate the quartz OSL signal from the whole rock slices by using IR and pulsed OSL (POSL) stimulations successively. It is known that the pulsed OSL characteristics of quartz and feldspars are very different (e.g. Denby et al., 2006). Thus, to isolate the quartz signal from our polymineral rock slices, we evaluated all 30 cobbles in a rapid screening test, where one slice from each rock was measured using both the IRSL and post-IR POSL signals in the same measurement cycle (Table S1). The post-IR POSL signals from samples with significant IRSL signals were generally decaying much more slowly than the corresponding signals from samples with negligible IRSL signals, indicating that the latter samples had smaller amounts of feldspar, and so were more likely for their post-IR POSL signal to predominantly originate from quartz (Fig. S1).

Based on a qualitative assessment of the shape of the post-IR POSL signals, the aliquots were grouped as per the degree of feldspar contamination in quartz OSL, including two samples with very low contamination, identified as quartz-rich and suitable for further measurements with the conventional CW OSL signal, and 10 samples characterized as feldspar-rich and suitable for measurement with CW IRSL signal. The remaining 17 samples with low- to moderate feldspar contamination of OSL signals were selected for measurements using the post-IR POSL signal.

Bleaching with depth

Guided by the screening results and the relative sensitivity of the samples to IR or blue light stimulation, the luminescence-depth profiles were determined by measuring the OSL, IRSL or post-IR (P)OSL natural sensitivity-corrected signals (i.e. L_n/T_n values) with depth in the two tabular sides of 36 cobbles, and one side of two cobbles. None of the observed $pIRIR_{225}$ profiles (measured as part of the post-IR POSL protocol) had the sigmoidal shape characteristic for well-bleached rock samples, and so this signal was not included in any further analysis.

Profiles of 24 of the 38 cobbles showed consistent L_n/T_n ratios from the surface to the depth, indicating that these cobbles had no light exposure before burial, and that their luminescence signals are in field saturation. Profiles of another 11 cobbles showed reduced L_n/T_n values near the surface but no near-surface plateaus, indicating that these cobbles were exposed to some light, but not enough to be sufficiently bleached (Fig. S2). Three cobbles (C-3, C-4 and C-1-11) contained, at least in one side, profiles with sigmoidal shapes typical for well-bleached rock surfaces, starting from small values near the surface and slowly rising towards saturation in depth (Fig. 2B).

In order to determine the extent of bleaching is these samples prior to burial, the observed IRSL (samples C-3 and C-4) and post-IR POSL (sample C-1-11) L_n/T_n values were first fitted (solid lines in Fig. 2B) using the model representing an exposure event followed by a burial event, which is the expected depositional history for these cobbles:

$$L(x) = L_0(x)\left(\left(e^{-\overline{\sigma\varphi_0}t_e e^{-\mu x}} - 1\right)e^{-\frac{\dot{D}}{D_0}t_b} + 1\right) \quad (1)$$

where L_0 is the initial luminescence signal before burial, $\overline{\sigma\varphi_0}$ (ka^{-1}) is the luminescence bleaching rate at the surface of the rock, t_e (ka) is the duration of the exposure time before burial, μ (mm^{-1}) is the coefficient of light attenuation into the rock, $\dot{D}$ ($Gy.ka^{-1}$) is the dose rate during burial, D_0 (Gy) is the characteristic dose and t_b (ka) is the burial time (Sohbati et al., 2015; Freiesleben et al., 2015).

The product terms $\overline{\sigma\varphi_0}t_e$ and $\dot{D}/D_0\, t_b$ are treated as single parameters in the fitting. This is because without independent knowledge of the value of $\overline{\sigma\varphi_0}$ or t_e, one cannot meaningfully treat them as separate parameters for the fitting. Also, the fitted value of t_b is not of interest, as it is directly derived from the D_e distribution of the surface slices. The resulting best-fit parameter values were then replaced in the following model for one exposure event only, to predict the shape of the profiles at the time of burial (dashed lines in Fig. 2B):

$$L(x) = L_0(x)e^{-\overline{\sigma\varphi_0}t_e e^{-\mu x}} \quad (2)$$

After Souza et al. (2021) we define a surface as well-bleached if the ratio of the predicted pre-burial profile to the observed post-burial profile is < 5%. The bottom side of C-3, the top surface of C-4, and both sides of C-1-11 are identified as well-bleached prior to burial (Fig. 2B, C). Having established the bleaching depth in these cobbles (Fig. 2C), additional cores, totalling at least 11, were cut from the well-bleached surfaces for D_e measurements and age determination.

Dose recovery

Prior to D_e measurements, the reliability of the IRSL (samples C-3 and C-4) and post-IR POSL (sample C-1-11) protocols (Table S1) was evaluated by dose recovery tests. For each protocol, six inner slices were optically bleached for 48 h (24 h each side) using a Hönle SOL2 solar simulator. Three of these were then measured using the protocol in question, while the remaining three slices were given a known dose in the laboratory and then measured in the same manner. The dose recovery ratios were calculated by taking the ratio of the measured dose subtracted by the residual dose to the given dose. The average IRSL dose recovery ratios for samples C-3 and C-4 was 0.94 ± 0.07 (n = 3), while the post-IR POSL ratio for sample C-1-11 was 0.96 ± 0.04 (n = 3). All these ratios are within 10% from unity indicating that our protocols can reliably recover a known dose in the laboratory (Murray and Wintle, 2003).

ENVIRONMENTAL DOSE RATES

Dose rate modelling

To derive the effective dose rate to the surface of the cobbles, the variation of beta and gamma dose rates at the pebble-matrix interface must be taken into account. Following Sohbati et al. (2015), and based on the superposition principle (Aitken, 1985; Appendix H), the gradient of beta dose rate with depth into the pebble can be expressed as:

$$\dot{D}_{\beta,total} = 0.5\dot{D}_{\beta,sed}e^{-bx} + \dot{D}_{\beta,rock}(1 - 0.5e^{-bx}) \quad (3)$$

where $\dot{D}_{\beta,sed}$ (Gy.ka^{-1}) and $\dot{D}_{\beta,rock}$ (Gy.ka^{-1}) are sediment and rock infinite matrix beta dose rates, respectively, b (mm^{-1}) is the linear beta attenuation coefficient into the pebble and x (mm) is depth. $\dot{D}_{\beta,sed}$ is corrected for water content and porosity of the matrix. The porosity of the sediment matrix was estimated to be 17% (Table S2). The value of b was calculated to be ~3.6 mm^{-1}, by taking the average of the attenuation coefficients for ^{238}U, ^{232}Th and ^{40}K decay series for sediment by Riedesel and Autzen (2020) (their best-fit values for single exponential fits) weighted by the activity concentrations in our samples (Table S2) and scaled for a density of 2.6 g.cm^{-3} for the cobbles. Figure S3 shows the variation of sediment, cobble, and total beta dose rates with depth for individual cobbles. The fraction of infinite matrix gamma dose rate absorbed by each cobble was calculated after Aitken (1985, Appendix H) using the empirical relationship $p = 2.6d\%$, where d (cm) is the diameter of the cobble. The effective total dose rate (excluding the internal beta dose rate due to ^{40}K content of the K-rich feldspar grains) to the surface slices from the cobbles was calculated by integrating the total dose rate over the thickness of the slices (i.e. < 3 mm depth into the rock).

Internal dose rate to K-rich feldspar grains in C-3 and C-4

The IRSL signal from feldspar mainly originates from K-rich areas in feldspar grains (Smedley et al., 2012). It is also known that the internal beta dose rate in K-rich feldspar grains is strongly dependent on the grain size due to the internal ^{40}K content (e.g. Smedley et al., 2012; Sohbati et al., 2013). The SEM-EDX maps of polished thin sections show that minerals with significant proportions of potassium (K-feldspar and muscovite) account for 32% and 10% of rocks C-3 and C-4, respectively. The grain-size distributions of these two minerals were calculated from maps of those minerals (Fig. S4). These data show the modal grain sizes of both K-feldspar and muscovite are ~90 µm in C-3 and 30 µm in C-4.

The relationship between grain size and internal beta dose rate due to ^{40}K and the associated ^{87}Rb content (Mejdahl, 1987) can well be assumed to be linear over such small ranges of grain size (i.e. < 100 µm) (Mejdahl, 1979; Readhead, 2002). In order to derive the internal beta dose rate to the average grain sizes estimated above, we calculated the absorbed ^{40}K and ^{87}Rb beta dose rate fractions using the empirical relationships by Mejdahl (1979) and Readhead (2002) for quartz grains, and adapted them for K-rich feldspar grains, assuming a homogenous K content of 12.5 ± 0.5% (Huntley and Baril, 1997) and a homogenous Rb content of 400 ± 100 ppm (Huntley and Hancock, 2001). The average internal beta dose rate for C-3 and C-4 are 0.136 ± 0.009 $Gy.ka^{-1}$ and 0.385 ± 0.021 $Gy.ka^{-1}$, respectively. These values are included in the total effective dose rates used for age calculation (Table S2).

FADING CORRECTION OF IRSL AGES

It is known that the IRSL signal from feldspars is unstable and gradually reduces over time due to a phenomenon known as anomalous fading (Wintle, 1973). The IRSL ages should thus be corrected by taking the loss of the IRSL signal into account. We followed two different approaches to correct the IRSL ages of C-3 and C-4.

g-value fading correction

The conventional method for fading correction is to characterise the rate of anomalous fading on a laboratory timescale in terms of a factor called the *g*-value (Aitken, 1985:

appendix F; Huntley and Lamothe, 2001). This value expresses the fading rate as a percentage of signal lost during a storage period of one decade of time, where the storage periods are expressed as decades relative to the laboratory irradiation time (Aitken, 1985: appendix F; Huntley and Lamothe, 2001). The *g*-value is estimated by measuring the IRSL signal reduction with storage time after irradiation (Auclair et al., 2003).

Following Auclair et al. (2003), we measured the fading rate on two slices from each cobble. The time spans between the irradiations and IRSL measurements were 0.11 h and 12 h for the prompt and delay measurements, respectively (Auclair et al., 2003). The regeneration and test doses were ~60 and 12 Gy, respectively. The *g*-values for individual aliquots were calculated following Huntley and Lamothe (2001) (Fig. S5). The average measured *g*-values are 3.19 ± 0.07 % decade^{-1} (n = 2) for C-3 and 4.23 ± 0.27 % decade^{-1} (n = 2) for C-4 (Table 1).

Field to laboratory saturation (FLS) ratio fading correction

One of the advantages of rock surface luminescence dating over the conventional sediment dating is that rocks contain a record of signal saturation in nature (so-called field saturation). This is the equilibrium level at which the signal growth rate due to dose rate and the signal loss rate because of anomalous fading are equal. In rocks, the field saturation limit can be inferred from the L_n/T_n values of slices from deep unexposed parts of the cobbles. Based on this, Rades et al. (2018) proposed an alternative approach of fading correction for rock samples. In this method, the field saturation limit (i.e. L_n/T_n values measured from deep unexposed slices) is divided by the laboratory saturation limit (i.e. L_x/T_x values measured from the same slices immediately after large saturating doses) to yield the field to laboratory saturation (FLS) ratio as an upper estimate of fading in a given rock sample. The larger the fading rate, the lower the field saturation limit, and the smaller the FLS ratio. In the low dose (more linear) part of the growth curve, the corrected age can thus be derived by dividing the uncorrected age by the FLS ratio (Rades et al., 2018).

To derive an average estimate of both field and laboratory saturation limits in C-3 and C-4, we selected three inner slices from each cobble whose L_n/T_n values were already measured to be in field saturation (i.e. they were lying on the plateau part of the corresponding luminescence depth profile; Fig. 2B). We then measured the response of each slice to a wide range of doses up to saturation to determine the laboratory saturation limit (i.e. the amplitude of the dose response curve; Fig. S6). For each cobble, the field saturation limit was calculated by averaging the L_n/T_n values from these three slices, and the laboratory saturation limit was determined by averaging the amplitude of the saturating dose response curve from the same slices (Fig. S6). These estimates of saturation limits were then divided to yield the FLS ratios of 0.74 ± 0.03 (n = 3) and 0.71 ± 0.03 (n = 3) for C-3 and C-4, respectively (Fig. S6).

SUPPLEMENTARY FIGURE CAPTIONS

Figure S1 – (A) Typical IRSL and post-IR OSL stimulation curves from sample C-4 compared with a post-IR OSL curve from a sensitised slice of quartzite used for calibration. (B) A typical post-IR POSL signal from sample C-1-11 compared with the corresponding signal from a sensitised slice of calibration quartzite; cts = counts.

Figure S2 – Typical luminescence depth profiles for (A) an unbleached cobble and (B) a partially bleached cobble. Our interpretations of whether the surfaces are at field saturation (no light), partially bleached (some light), or bleached are shown for each rock surface.

Figure S3 – Variation of sediment, cobble, and total beta dose rate with depth into individual cobbles.

Figure S4 – Cumulative size distributions of grain-sizes of (a) K-feldspar and (b) muscovite for rocks C-3 and C-4 determined by mineral scanning using SEM-EDX.

Figure S5 – Typical g-value measurement on a rock slice from sample C-3 (left panel) and C-4 (right panel). The shaded area depicts the 95% confidence band.

Figure S6 – Average dose response curves (solid lines) for samples C-3 (left panel) and C-4 (right panel) measured from three inner slices from the unexposed parts of the cobbles. For each sample, the field saturation limit (dashed line) is derived by averaging the natural signals from the slices (i.e. L_n/T_n values represented by open squares on the y-axes), while the laboratory saturation (dash-dotted line) is determined by the amplitude of the average dose response curve. The field to laboratory saturation ratios (shown next to the down arrows) provide an upper limit for signal instability in nature.

SUPPLEMENTARY TABLES

Table S1: Outline of the Single-Aliquot Regenerative dose (SAR) protocols used in this study.

Table S2: Summary of cobble size, grain size, radionuclide concentrations (dry material), estimated water-content and porosity values, and calculated dose rates.

REFERENCES CITED

Aitken, M.J., 1985, Thermoluminescence Dating: London, Academic Press, 359 p.

Auclair, M., Lamothe, M., and Huot, S., 2003, Measurement of anomalous fading for feldspar IRSL using SAR: Radiation Measurements, v. 37, p. 487–492, doi:10.1016/S1350-4487(03)00018-0.

Banerjee, D., Murray, A.S., Bøtter-Jensen, L., and Lang, A., 2001, Equivalent dose estimation using a single aliquot of polymineral fine grains: Radiation Measurements, v. 33, p. 73–94, doi:10.1016/S1350-4487(00)00101-3.

Denby, P.M., Bøtter-Jensen, L., Murray, A.S., Thomsen, K.J., and Moska, P., 2006, Application of pulsed OSL to the separation of the luminescence components from a mixed quartz/feldspar sample: Radiation Measurements, v. 41, p. 774–779, doi:10.1016/J.RADMEAS.2006.05.017.

Duller, G.A.T., 2003, Distinguishing quartz and feldspar in single grain luminescence measurements: Radiation Measurements, v. 37, p. 161–165, doi:10.1016/S1350-4487(02)00170-1.

Freiesleben, T., Sohbati, R., Murray, A.S., Jain, M., al Khasawneh, S., Hvidt, S., and Jakobsen, B., 2015, Mathematical model quantifies multiple daylight exposure and burial events for rock surfaces using luminescence dating: Radiation Measurements, v. 81, p. 1–7, doi:10.1016/j.radmeas.2015.02.004.

Guérin, G., Mercier, N., and Adamiec, G., 2011, Dose-rate conversion factors: update: Ancient TL, v. 29, p. 5–8, http://www.aber.ac.uk/temp-ancient-tl/issue16_2/adamiec_atl_16(2)_37-50.pdf.

Huntley, D., and Baril, M., 1997, The K content of the K-feldspars being measured in optical dating or in thermoluminescence dating: Ancient TL, v. 15, p. 11–13, http://www.sfu.ca/physics/research/workarea/huntley/98paper.pdf%5Cnhttp://www.aber.ac.uk/temp-ancient-tl/issue15_1/huntley_atl_15(1)_11-13.pdf.

Huntley, D.J., and Hancock, R.G.V., 2001, The Rb contents of the K-feldspars being measured in optical dating: Ancient TL, v. 19, p. 43–46.

Huntley, D.J., and Lamothe, M., 2001, Ubiquity of anomalous fading in K-feldspars and the measurement and correction for it in optical dating: Canadian Journal of Earth Sciences, v. 38, p. 1093–1106, doi:10.1139/cjes-38-7-1093.

Jutzeler, M., Proussevitch, A.A., and Allen, S.R., 2012, Grain-size distribution of volcaniclastic rocks 1: A new technique based on functional stereology: Journal of Volcanology and Geothermal Research, v. 239–240, p. 1–11, doi:10.1016/j.jvolgeores.2012.05.013.

Lapp, T., Kook, M., Murray, A.S., Thomsen, K.J., Buylaert, J.P., and Jain, M., 2015, A new luminescence Detection and Stimulation Head for the Risø TL/OSL reader: Radiation Measurements, v. 81, p. 178–184, doi:10.1016/j.radmeas.2015.02.001.

Liu, J., Murray, A., Sohbati, R., and Jain, M., 2016, The effect of test dose and first IR stimulation temperature on post-IR IRSL measurements of rock slices: Geochronometria, v. 43, p. 179–187, doi:10.1515/GEOCHR-2015-0049.

Mejdahl, V., 1979, Thermoluminescence dating: Beta-dose attenuation in quartz grains: Archaeometry, v. 21, p. 61–72, doi:10.1111/j.1475-4754.1979.tb00241.x.

Mejdahl, V., 1987, Internal radioactivity in quartz and feldspar grains: Ancient TL, v. 5, p. 10–17.

Mooneyham, C., and Strom, K., 2018, Deposition of Suspended Clay to Open and Sand-Filled Framework Gravel Beds in a Laboratory Flume: Water Resources Research, v. 54, p. 323–344, doi:10.1002/2017WR020748.

Murray, A.S., and Wintle, A.G., 2000, Luminescence dating of quartz using an improved single-aliquot regenerative-dose protocol: Radiation Measurements, v. 32, p. 57–73, doi:10.1016/S1350-4487(99)00253-X.

Murray, A.S., and Wintle, A.G., 2003, The single aliquot regenerative dose protocol: potential for improvements in reliability: Radiation Measurements, v. 37, p. 377–381, doi:10.1016/S1350-4487(03)00053-2.

Murray, A.S., Helsted, L.M., Autzen, M., Jain, M., and Buylaert, J.P., 2018, Measurement of natural radioactivity: Calibration and performance of a high-resolution gamma spectrometry facility: Radiation Measurements, doi:10.1016/j.radmeas.2018.04.006.

Rades, E.F.F., Sohbati, R., Lüthgens, C., Jain, M., and Murray, A.S.S., 2018, First luminescence-depth profiles from boulders from moraine deposits: Insights into glaciation chronology and transport dynamics in Malta valley, Austria: Radiation Measurements, v. 120, p. 281–289, doi:10.1016/J.RADMEAS.2018.08.011.

Readhead, M.L., 2002, Absorbed dose fraction for 87Rb β particles: Ancient TL, v. 20, p. 25–28.

Riedesel, S., and Autzen, M., 2020, Beta and gamma dose rate attenuation in rocks and sediment: Radiation Measurements, v. 133, p. 106295, doi:10.1016/j.radmeas.2020.106295.

Schneider, C.A., Rasband, W.S., and Eliceiri, K.W., 2012, NIH Image to ImageJ: 25 years of image analysis: Nature Methods, v. 9, p. 671–675, doi:10.1038/nmeth.2089.

Smedley, R.K., Duller, G.A.T., Pearce, N.J.G., and Roberts, H.M., 2012, Determining the K-content of single-grains of feldspar for luminescence dating, *in* Radiation Measurements, Pergamon, v. 47, p. 790–796, doi:10.1016/j.radmeas.2012.01.014.

Sohbati, R., Murray, A., Jain, M., Thomsen, K., Hong, S.C., Yi, K., and Choi, J.H., 2013, Na-rich feldspar as a luminescence dosimeter in infrared stimulated luminescence (IRSL) dating: Radiation Measurements, v. 51–52, p. 67–82, http://www.sciencedirect.com/science/article/pii/S1350448712003605?via%3Dihub (accessed September 2017).

Sohbati, R., Murray, A., Lindvold, L., Buylaert, J.P., and Jain, M., 2017, Optimization of laboratory illumination in optical dating: Quaternary Geochronology, v. 39, p. 105–111, doi:10.1016/j.quageo.2017.02.010.

Sohbati, R., Murray, A.S., Buylaert, J.P., Almeida, N.A.C., and Cunha, P.P., 2012, Optically stimulated luminescence (OSL) dating of quartzite cobbles from the Tapada do Montinho archaeological site (east-central Portugal): Boreas, v. 41, p. 452–462, doi:10.1111/j.1502-3885.2012.00249.x.

Sohbati, R., Murray, A.S., Jain, M., Buylaert, J.-P.P., and Thomsen, K.J., 2011, Investigating the resetting of osl signals in rock surfaces: Geochronometria, v. 38, p. 249–258, doi:10.2478/s13386-011-0029-2.

Sohbati, R., Murray, A.S., Porat, N., Jain, M., and Avner, U., 2015, Age of a prehistoric “Rodedian” cult site constrained by sediment and rock surface luminescence dating techniques: Quaternary Geochronology, v. 30, p. 90–99, doi:10.1016/j.quageo.2015.09.002.

Souza, P.E., Sohbati, R., Murray, A.S., Clemmensen, L.B., Kroon, A., and Nielsen, L., 2021, Optical dating of cobble surfaces determines the chronology of Holocene beach ridges in Greenland: Boreas, p. 1–13, doi:10.1111/bor.12507.

Tsukamoto, S., and Rades, E.F., 2016, Performance of pulsed OSL stimulation for minimising the feldspar signal contamination in quartz samples: Radiation Measurements, v. 84, p. 26–33, doi:10.1016/j.radmeas.2015.11.007.

Wintle, A.G., 1973, Anomalous Fading of Thermo-luminescence in Mineral Samples: Nature, v. 245, p. 143–144, doi:10.1038/245143a0.

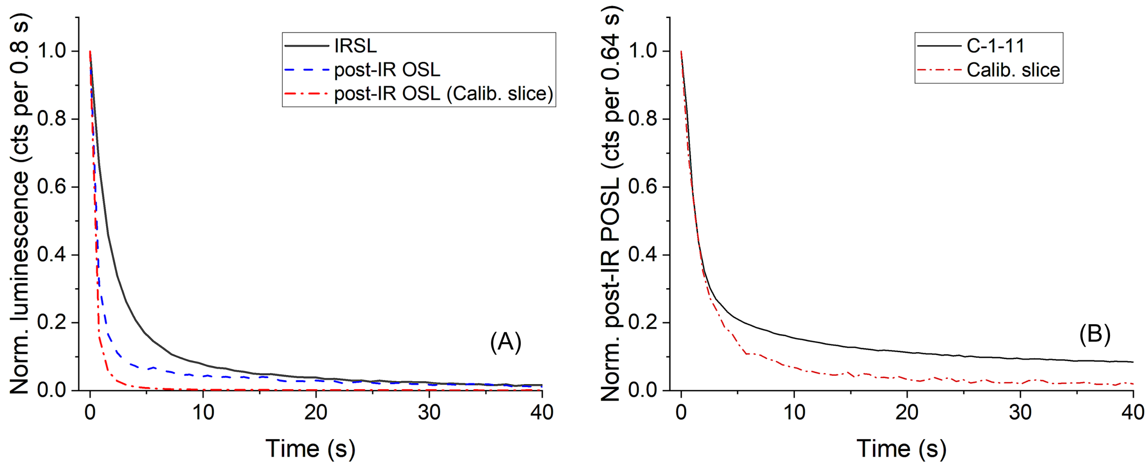
Norm. luminescence (cts per 0.8 s)
1.0
0.8
0.6
0.4
0.2
0.0
0
10
20
30
40
Time (s)
IRSL
post-IR OSL
post-IR OSL (Calib. slice)
(A)
Norm. post-IR POSL (cts per 0.64 s)
C-1-11
Calib. slice
(B)

Fig. S1

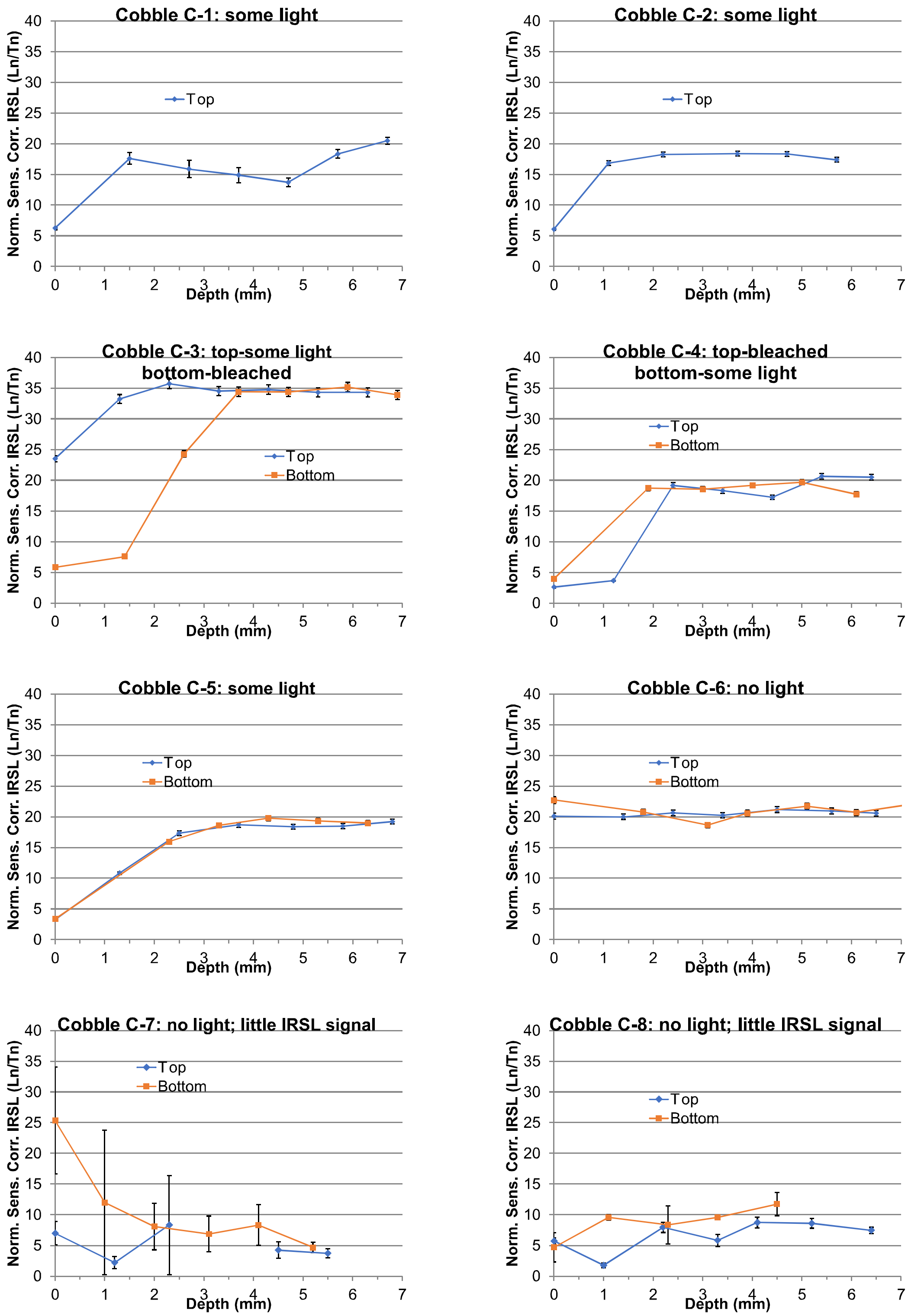
Cobble C-1: some light
Norm. Sens. Corr. IRSL (Ln/Tn)
Depth (mm)
Top
Cobble C-2: some light
Cobble C-3: top-some light
bottom-bleached
Bottom
Cobble C-4: top-bleached
bottom-some light
Cobble C-5: some light
Cobble C-6: no light
Cobble C-7: no light; little IRSL signal
Cobble C-8: no light; little IRSL signal

Fig. S2

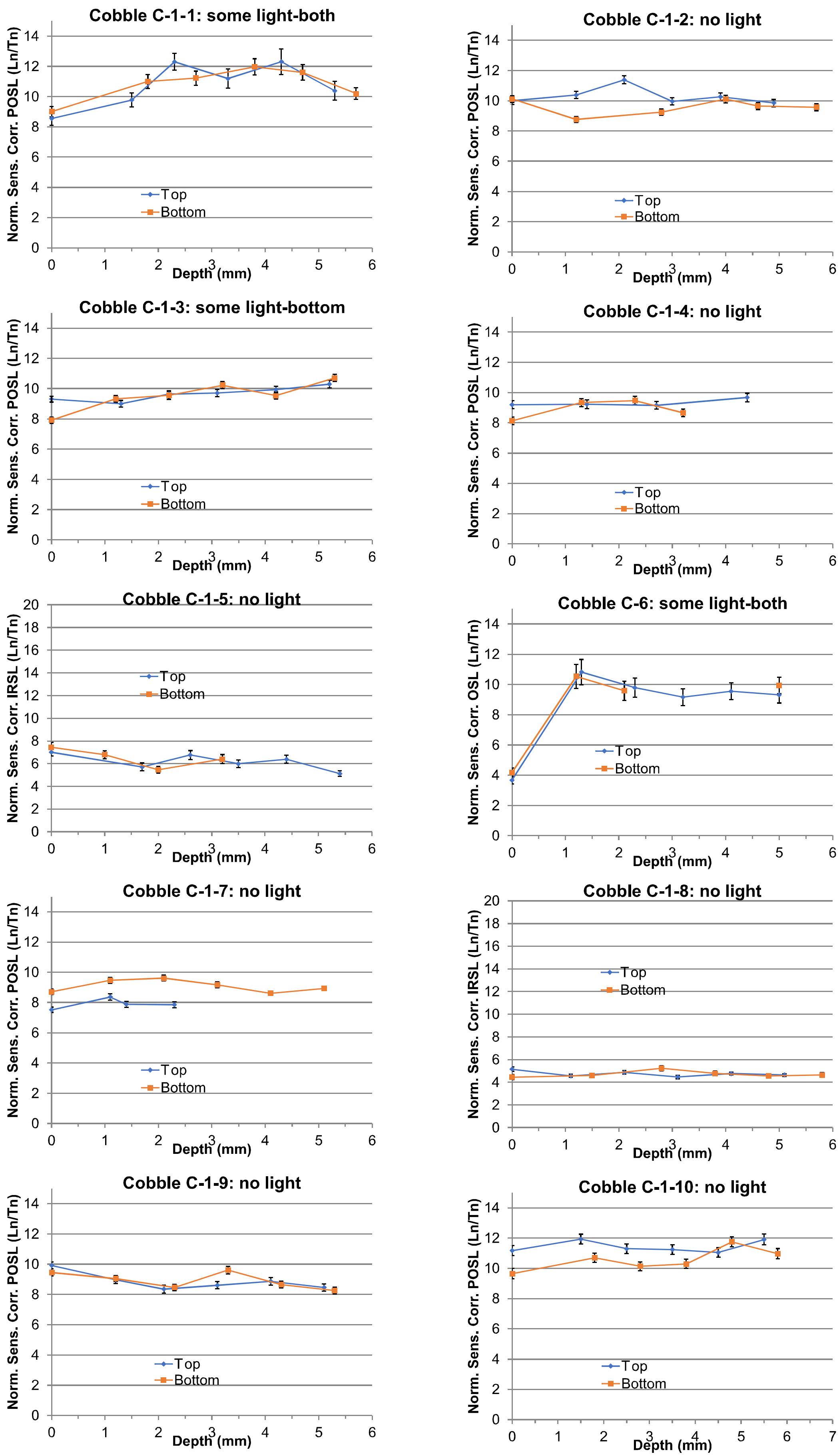
Cobble C-1-1: some light-both
Norm. Sens. Corr. POSL (Ln/Tn)
Depth (mm)
Top
Bottom
Cobble C-1-2: no light
Norm. Sens. Corr. POSL (Ln/Tn)
Depth (mm)
Top
Bottom
Cobble C-1-3: some light-bottom
Norm. Sens. Corr. POSL (Ln/Tn)
Depth (mm)
Top
Bottom
Cobble C-1-4: no light
Norm. Sens. Corr. POSL (Ln/Tn)
Depth (mm)
Top
Bottom
Cobble C-1-5: no light
Norm. Sens. Corr. IRSL (Ln/Tn)
Depth (mm)
Top
Bottom
Cobble C-6: some light-both
Norm. Sens. Corr. OSL (Ln/Tn)
Depth (mm)
Top
Bottom
Cobble C-1-7: no light
Norm. Sens. Corr. POSL (Ln/Tn)
Depth (mm)
Top
Bottom
Cobble C-1-8: no light
Norm. Sens. Corr. IRSL (Ln/Tn)
Depth (mm)
Top
Bottom
Cobble C-1-9: no light
Norm. Sens. Corr. POSL (Ln/Tn)
Depth (mm)
Top
Bottom
Cobble C-1-10: no light
Norm. Sens. Corr. POSL (Ln/Tn)
Depth (mm)
Top
Bottom

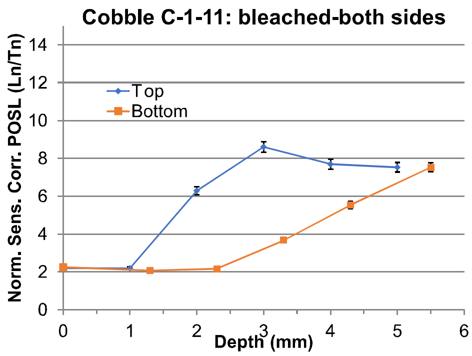
Cobble C-1-11: bleached-both sides
Norm. Sens. Corr. POSL (Ln/Tn)
Depth (mm)
Top
Bottom

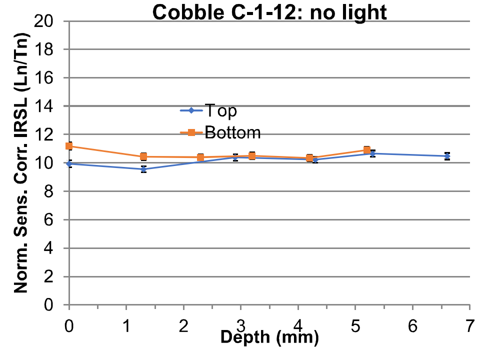
Cobble C-1-12: no light
Norm. Sens. Corr. IRSL (Ln/Tn)
Depth (mm)
Top
Bottom

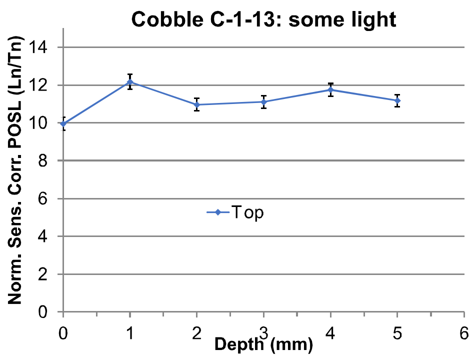
Cobble C-1-13: some light
Norm. Sens. Corr. POSL (Ln/Tn)
Depth (mm)
Top

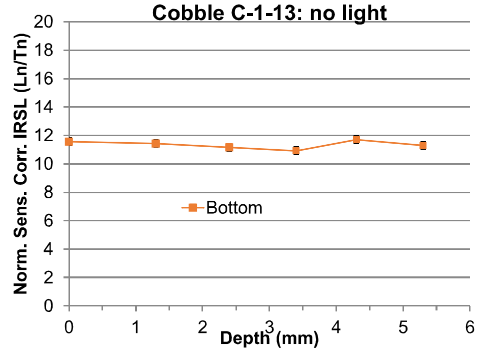
Cobble C-1-13: no light
Norm. Sens. Corr. IRSL (Ln/Tn)
Depth (mm)
Bottom

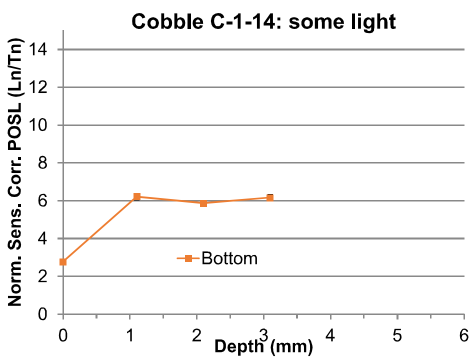
Cobble C-1-14: some light
Norm. Sens. Corr. POSL (Ln/Tn)
Depth (mm)
Bottom

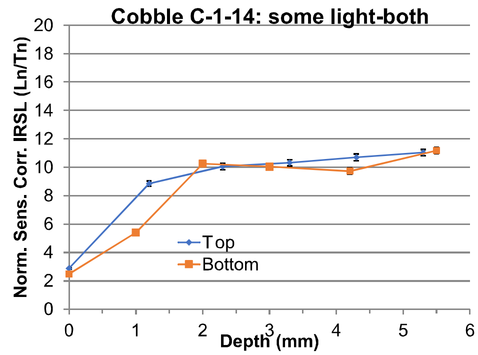
Cobble C-1-14: some light-both
Norm. Sens. Corr. IRSL (Ln/Tn)
Depth (mm)
Top
Bottom

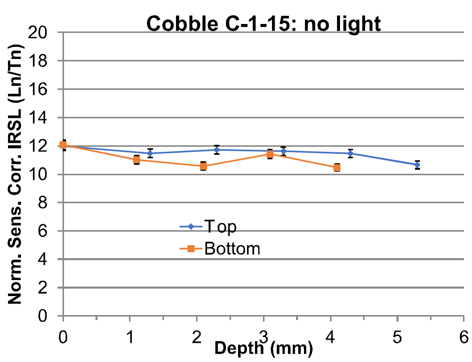
Cobble C-1-15: no light
Norm. Sens. Corr. IRSL (Ln/Tn)
Depth (mm)
Top
Bottom

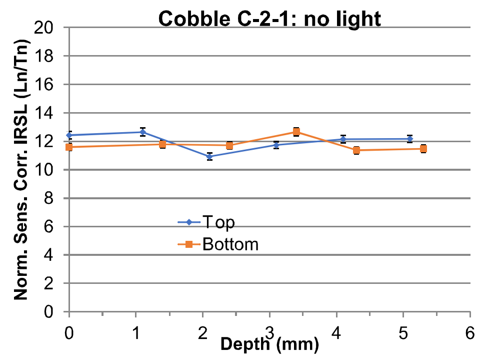
Cobble C-2-1: no light
Norm. Sens. Corr. IRSL (Ln/Tn)
Depth (mm)
Top
Bottom

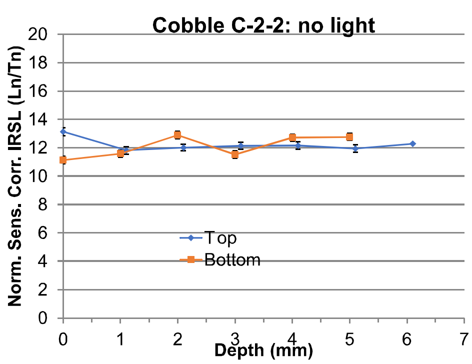
Cobble C-2-2: no light
Norm. Sens. Corr. IRSL (Ln/Tn)
Depth (mm)
Top
Bottom

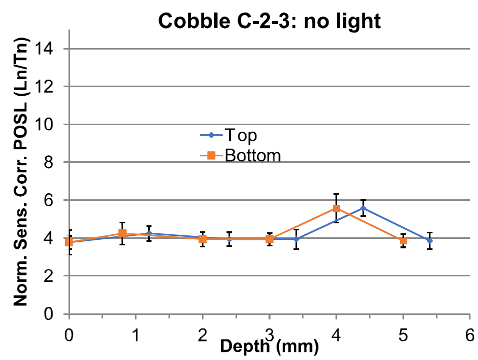
Cobble C-2-3: no light
Norm. Sens. Corr. POSL (Ln/Tn)
Depth (mm)
Top
Bottom

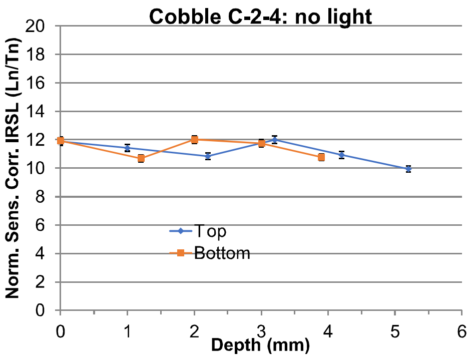
Cobble C-2-4: no light
Norm. Sens. Corr. IRSL (Ln/Tn)
Depth (mm)
Top
Bottom

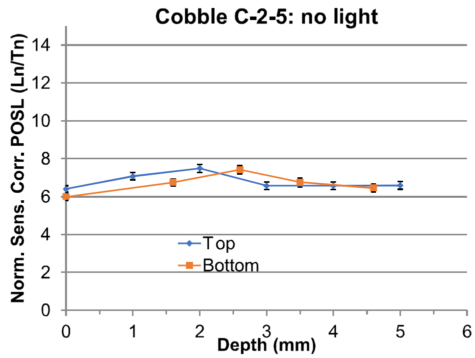
Cobble C-2-5: no light
Norm. Sens. Corr. POSL (Ln/Tn)
Depth (mm)
Top
Bottom

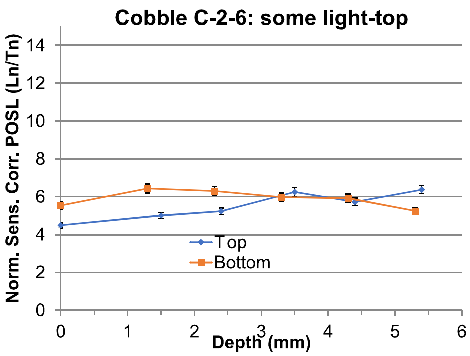
Cobble C-2-6: some light-top
Norm. Sens. Corr. POSL (Ln/Tn)
Depth (mm)
Top
Bottom

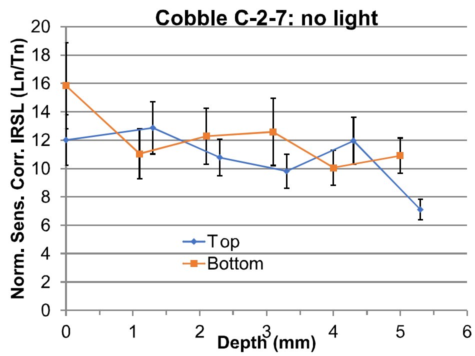
Cobble C-2-7: no light
Norm. Sens. Corr. IRSL (Ln/Tn)
Depth (mm)
Top
Bottom

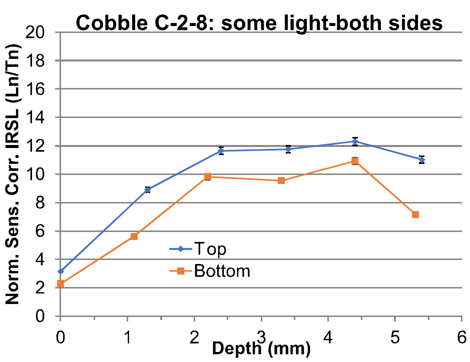
Cobble C-2-8: some light-both sides
Norm. Sens. Corr. IRSL (Ln/Tn)
Depth (mm)
Top
Bottom

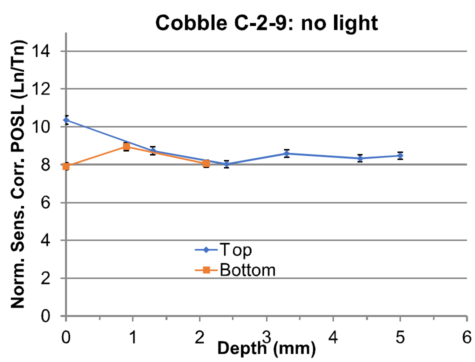
Cobble C-2-9: no light
Norm. Sens. Corr. POSL (Ln/Tn)
Depth (mm)
Top
Bottom

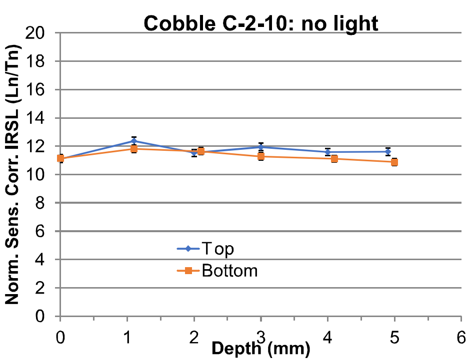
Cobble C-2-10: no light
Norm. Sens. Corr. IRSL (Ln/Tn)
Depth (mm)
Top
Bottom

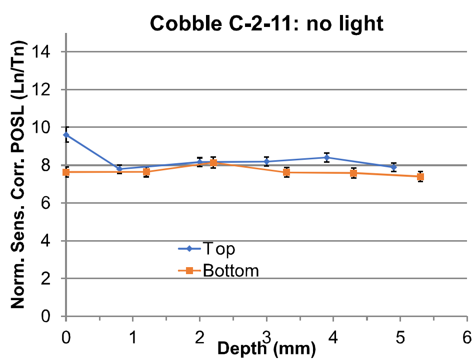
Cobble C-2-11: no light
Norm. Sens. Corr. POSL (Ln/Tn)
Depth (mm)
Top
Bottom

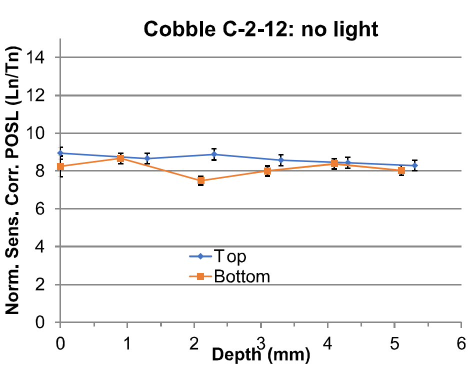
Cobble C-2-12: no light
Norm. Sens. Corr. POSL (Ln/Tn)
Depth (mm)
Top
Bottom

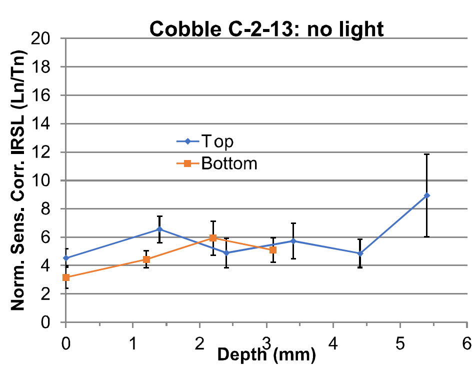
Cobble C-2-13: no light
Norm. Sens. Corr. IRSL (Ln/Tn)
Depth (mm)
Top
Bottom

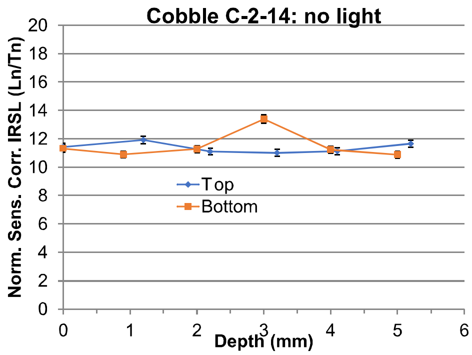
Cobble C-2-14: no light
Norm. Sens. Corr. IRSL (Ln/Tn)
Depth (mm)
Top
Bottom
0
2
4
6
8
10
12
14
16
18
20
0
1
2
3
4
5
6

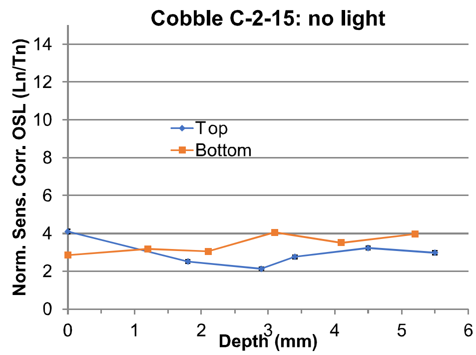
Cobble C-2-15: no light
Norm. Sens. Corr. OSL (Ln/Tn)
Depth (mm)
Top
Bottom
0
2
4
6
8
10
12
14
0
1
2
3
4
5
6

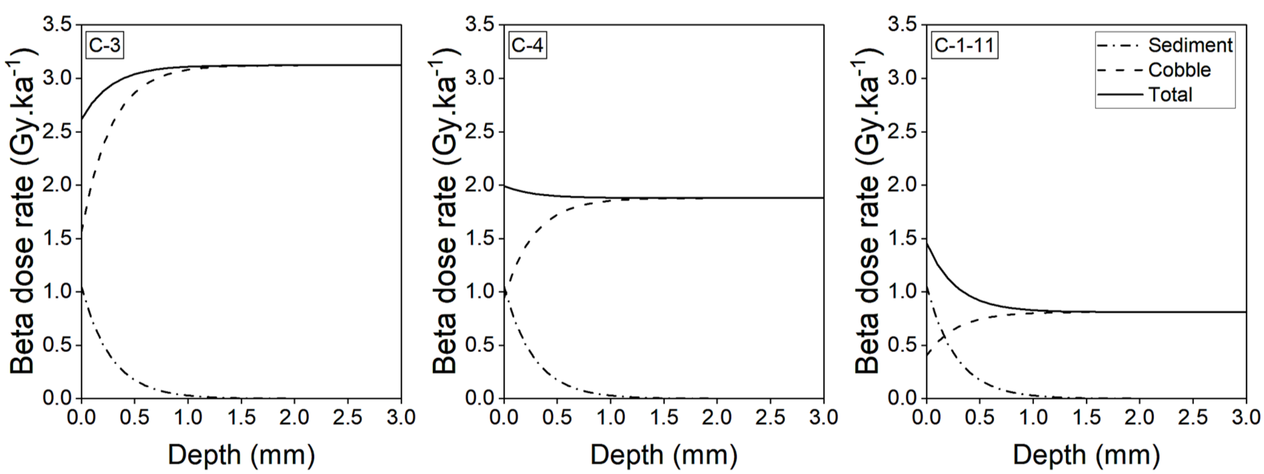
C-3
C-4
C-1-11
Sediment
Cobble
Total
Beta dose rate (Gy.ka-1)
Depth (mm)
0.0
0.5
1.0
1.5
2.0
2.5
3.0
3.5

Fig. S3

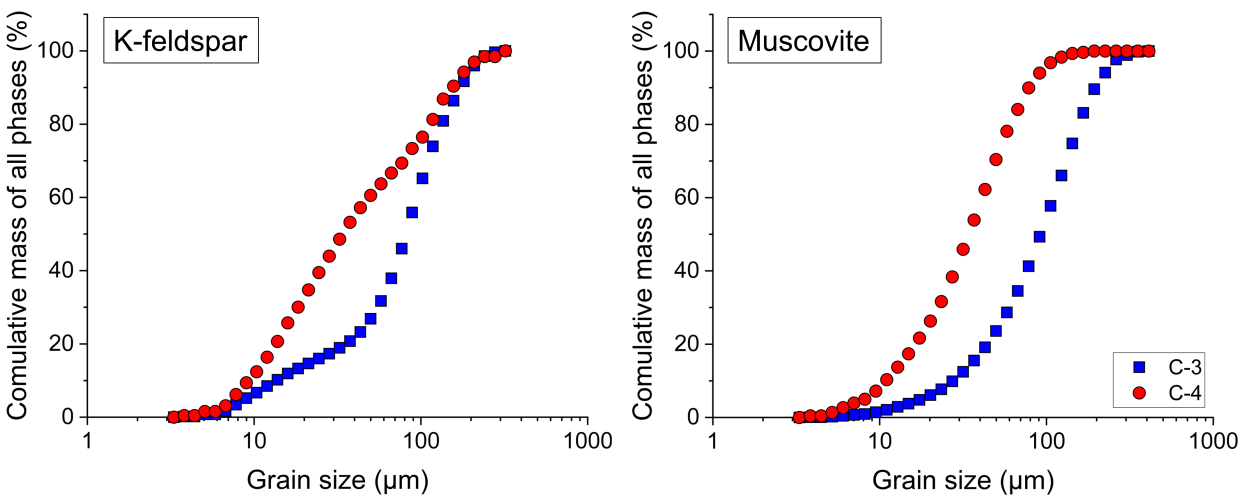
K-feldspar
Muscovite
Comulative mass of all phases (%)
Grain size (µm)
0
20
40
60
80
100
1
10
100
1000
C-3
C-4

Fig. S4

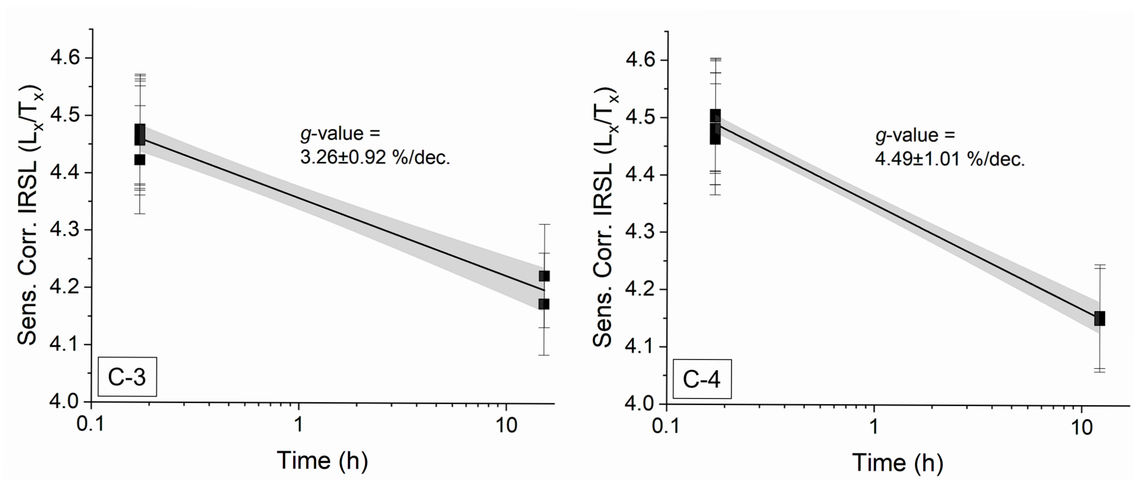
Sens. Corr. IRSL (L_x/T_x)
4.6
4.5
4.4
4.3
4.2
4.1
4.0
0.1
1
10
Time (h)
g-value =
3.26±0.92 %/dec.
C-3
Sens. Corr. IRSL (L_x/T_x)
g-value =
4.49±1.01 %/dec.
C-4
Time (h)

Fig. S5

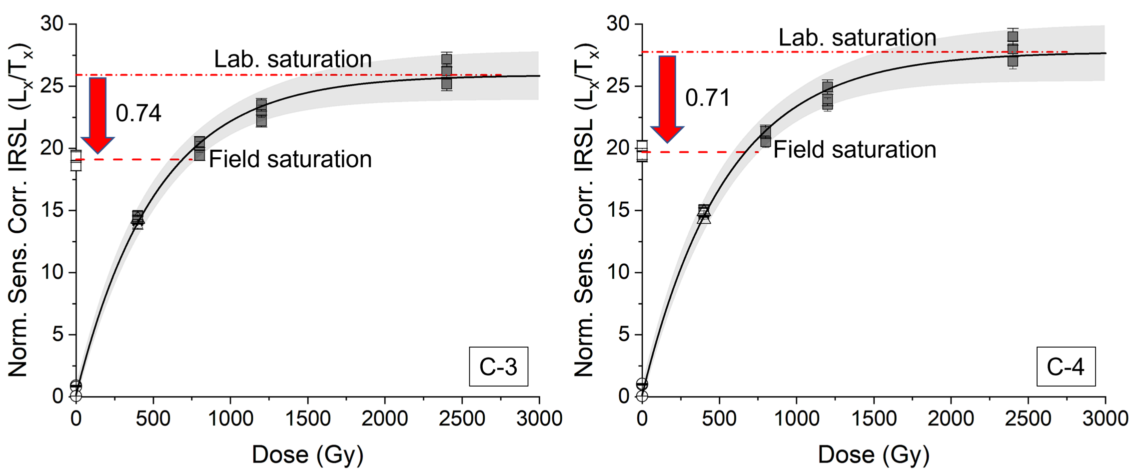
Lab. saturation
0.74
Field saturation
C-3
Norm. Sens. Corr. IRSL (L_x/T_x)
Dose (Gy)
Lab. saturation
0.71
Field saturation
C-4
Norm. Sens. Corr. IRSL (L_x/T_x)
Dose (Gy)

Fig. S6